The relation between dayside local Poynting flux enhancement and cusp reconnection

Wenhui Li,[1] Delores Knipp,[2,3] Jiuhou Lei,[3] and Joachim Raeder[1]

Received 15 February 2011; revised 19 May 2011; accepted 1 June 2011; published 5 August 2011.

[1] The Defense Meteorological Satellite Program (DMSP) F15 satellite frequently observes an unusually high level of local Poynting flux when the interplanetary magnetic field (IMF) is northward but also has a large B_y component. We use the Open Geospace General Circulation Model (OpenGGCM) coupled magnetosphere-ionosphere-thermosphere code to study several events where, under such conditions, unusually large earthward Poynting flux has been observed. We find that the Joule heating rate in the model agrees well with the observed Poynting flux. Analysis of the model results shows that the strong Poynting flux hot spots are physically linked with magnetic reconnection at the high-latitude cusps. The solar wind mechanical force and the $\mathbf{J} \times \mathbf{B}$ force act on the newly opened field lines created by cusp reconnection to produce a Pedersen current, which consequently generates an intense Joule heating region, and a pair of adjacent and opposite field-aligned currents (FACs) connecting to the magnetopause currents forming a closed circuit. The intense Joule heating region is also the region with strong downward Poynting flux. The distribution, scale, and magnitude of this Joule heating region and corresponding FACs in the polar regions are mainly controlled by IMF clock angle, IMF magnitude, and solar wind dynamic pressure. A northward IMF condition with a large B_y component will result in an extended region with intense Joule heating and FAC, thus making a spacecraft transiting the dayside region more likely to observe a strong downward Poynting flux.

Citation: Li, W., D. Knipp, J. Lei, and J. Raeder (2011), The relation between dayside local Poynting flux enhancement and cusp reconnection, *J. Geophys. Res.*, *116*, A08301, doi:10.1029/2011JA016566.

1. Introduction

[2] It is well known that the direction and strength of the interplanetary magnetic field (IMF) exert strong influences on the high-latitude ionospheric plasma convection and current [e.g., *Heppner*, 1972; *Heppner and Maynard*, 1987; *Foster et al.*, 1986; *Ruohoniemi and Greenwald*, 1996; *Weimer*, 1995, 2001]. Such influences are strongest when the IMF is southward. During a period of northward IMF conditions, the accepted view is that the magnetosphere becomes quiet, the open-closed boundary in the ionosphere shrinks, and the energy deposited into the ionosphere is reduced greatly, thus weakening ionospheric plasma convection and currents.

[3] However, using data from the DMSP F15 satellite with an altitude of 859 km, *Knipp et al.* [2011] recently found unusually high, localized Poynting flux enhancements in the dayside near-cusp region during periods of solar wind shocks with northward B_z and strong B_y conditions. The peak value of such downward Poynting flux can be up to 180 mW m^{-2}, while the typical maximum values are close to 40 mW m^{-2} during a moderate storm. Data from Dynamics Explorer 2 showed a peak value of ~50 mW m^{-2} after 2 h of strongly southward IMF [*Gary et al.*, 1994]. The corresponding assimilative mapping of ionospheric electrodynamics (AMIE) Joule heating map also shows a high Joule heating rate near the region of strong Poynting flux observation [*Crowley et al.*, 2010]. Using iridium magnetic data and a statistical ionospheric conductivity model, *Korth et al.* [2005] estimate the global distribution of radial Poynting flux showing a hot spot in the ionosphere poleward of 78° magnetic latitude with a maximum energy flux of near 50 mW m^{-2} during a period of strongly northward IMF conditions.

[4] *Crowley et al.* [2010] successfully reproduced the main features of the density enhancements observed by the Challenging Minisatellite Payload (CHAMP) satellite with an altitude of 363 km on 24 August 2005 using the Thermosphere Ionosphere Mesosphere Electrodynamics General Circulation Model (TIMEGCM), which was driven by high-fidelity, high-latitude inputs specified by the AMIE algorithm in the study instead of inputs from a simpler con-

[1]Space Science Center, University of New Hampshire, Durham, New Hampshire, USA.
[2]High Altitude Observatory, National Center for Atmospheric Research, Boulder, Colorado, USA.
[3]Department of Aerospace Engineering Sciences, University of Colorado at Boulder, Boulder, Colorado, USA.

0148-0227/11/2011JA016566

vection model [*Heelis et al.*, 1982]. Their simulations reveal that the observed density enhancement in the dayside cusp region resulted from large amounts of energy entering the ionosphere-thermosphere system at cusp latitudes during an interval of strong (+20 nT) IMF B_y with B_z fluctuating between +10 nT and −10 nT.

[5] Motivated by the new discovery made by *Knipp et al.* [2011] and the study of *Crowley et al.* [2010], we use the global magnetosphere MHD model Open Geospace General Circulation Model (OpenGGCM) [*Raeder et al.*, 1998, 2001; *Raeder*, 2003] coupled with the NOAA Coupled Thermosphere Ionosphere Model (CTIM) [*Fuller-Rowell et al.*, 1996] to simulate the events of strong Poynting flux. In this paper, we analyze the simulation results and reveal the mechanism that leads to the observations of strong Poynting flux under northward IMF conditions. This paper is organized as follows: In section 2 we discuss the OpenGGCM model and the data sources. Sections 3 through 5 provide examples of model-data comparisons for three events. We discuss the analysis results in section 6 and summarize our new findings in section 7.

2. Model and Data Sources

[6] OpenGGCM solves the resistive MHD equations on a nonuniform rectilinear grid with a minimum grid spacing at GSE $y = 0$ and $z = 0$ for the y and z directions and at a point near the dayside magnetopause for the x direction. The outer boundary conditions on the dayside are the solar wind and IMF conditions, while those on the other five outer boundaries are free (i.e., normal derivatives vanish). The inner boundary conditions are derived from an ionospheric model coupled with the magnetosphere model. FACs are computed just outside a spherical region of radius 3.0 R_E, centered around the Earth, and mapped to a spherical-polar ionosphere grid at 1.02 R_E using a dipole magnetic field model. The ionosphere potential is solved on the surface of a sphere with a 1.02 R_E radius. The ionospheric electric field is mapped outward to the surface of the sphere with a 3.0 R_E radius. In an OpenGGCM simulation, the ionosphere can be either set simply as a sphere with constant uniform conductance, modeled by empirical parameters [*Robinson et al.*, 1987] or modeled by the NOAA CTIM [*Fuller-Rowell et al.*, 1996]. A more detailed description of the OpenGGCM model and its ionosphere coupling can be found in related articles [*Raeder et al.*, 1998, 2001; *Raeder*, 2003].

[7] For this study, we use solar wind data from ACE to drive the simulation in a domain of GSE (−24, 650) × (−48, 48) × (−48, 48) R_E with a minimum grid size of 0.12 R_E and about 28 million grid points. The CTIM is used as the coupled ionosphere-thermosphere model. The grid distribution in this simulation is designed to put emphasis on the dayside and flanks. The magnetospheric parameter values (plasma density, temperature, velocity, magnetic field, and current density) of the whole domain are written out every 3 min, and the ionospheric parameter values (proton precipitation, electron precipitation, Pedersen conductance, Hall conductance, FAC, and Joule heating rate) are written out every minute. The values at a given position and time can be obtained from linear spatial and temporal interpolation for further analysis.

[8] The DMSP Poynting flux is computed by

$$\mathbf{E} = -\mathbf{V} \times \mathbf{B}_{main}, \tag{1}$$

$$\delta\mathbf{B}_{DMSPHorizontal} = \mathbf{B}_{\mathrm{DMSP}} - \mathbf{B}_{\mathrm{main}}, \tag{2}$$

$$\mathbf{S} = (\mathbf{E} \times \delta\mathbf{B}_{\mathrm{DMSPHorizontal}})/\mu_o, \tag{3}$$

where $\mathbf{V}$ is plasma velocity measured by the DMSP drift meter, $\mathbf{B}_{main}$ is the International Geomagnetic Reference Field main field, and $\mathbf{B}_{\mathrm{DMSP}}$ is the magnetic field measured by DMSP. The vertical Poynting flux is then given by

$$S_{\parallel} = \left(E_x \delta B_y - E_y \delta B_x\right)/\mu_o, \tag{4}$$

where the x component is along the spacecraft track and the y component is across the spacecraft track.

[9] For a stationary condition, Poynting's theorem relates the electromagnetic energy transfer rate $\mathbf{J} \cdot \mathbf{E}$ to the perturbation Poynting flux $\mathbf{S}$:

$$\mathbf{J} \cdot \mathbf{E} = -\nabla \cdot \mathbf{S}. \tag{5}$$

If, as discussed by *Richmond* [2010], Poynting's theorem and Gauss's theorem are applied to a single flux tube bounded by the satellite at the top and the base of ionosphere at the bottom, and assuming that no energy flows out of the bottom of the region, it is found that the Poynting flux $S_{\parallel}$ across the boundary is equal to minus the rate of energy conversion below [*Kelley et al.*, 1991; *Gary et al.*, 1994; *Deng et al.*, 2008]:

$$S_{\parallel} = -\int \mathbf{E} \cdot \mathbf{J} dh, \tag{6}$$

where the integral is from the bottom to the top of the boundary and the variation of the magnetic field along the flux tube is neglected.

[10] In OpenGGCM, the Joule heating rate on an ionospheric surface grid is computed by

$$hj = \mathbf{E} \cdot \int \mathbf{J} dh, \tag{7}$$

where the integral is from the bottom to the top of the ionosphere and $\mathbf{E}$ is assumed to be constant along the radial direction. Both $\mathbf{E}$ and $\mathbf{J}$ are provided by CTIM.

[11] In the high-latitude region, the dipole field is mostly radial, and if the variation of the ionospheric electric field along the height is neglected, the observed magnitude of the Poynting flux $S_{\parallel}$ should be approximately equal to the total Joule heating rate hj for the ionospheric volume below the spacecraft according to equations (6) and (7).

3. Event 24 August 2005

[12] Motivated by the event studied by *Crowley et al.* [2010], who suggested a connection between significant thermospheric density enhancement and greatly enhanced Poynting flux, we ran a simulation for this event. Figure 1 shows the DMSP F15 observation of downward Poynting flux, the corresponding Joule heating rate on the virtual

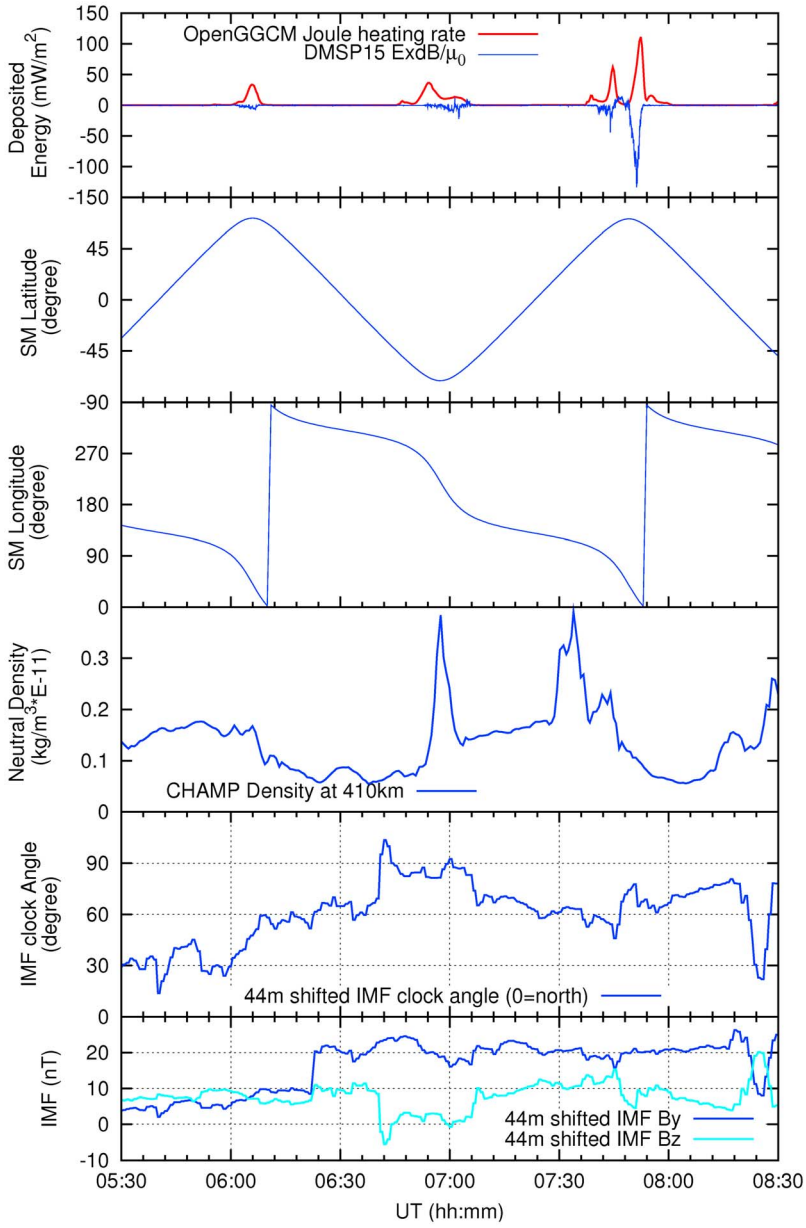

Figure 1. Observation and simulation results for 24 August 2005. From top to bottom are DMSP F15 observation of Poynting flux and the corresponding Joule heating rate on the virtual DMSP orbit in the simulation, DMSP latitude in solar magnetic (SM) coordinates, DMSP longitude in SM coordinates, CHAMP observation of neutral density, IMF clock angle (arctan(B_y/B_z)), and IMF y and z components derived from ACE measurements. The negative values of Poynting flux indicate the flux is directed earthward.

DMSP orbit in the simulation, the DMSP latitude and longitude in solar magnetic (SM) coordinates, the CHAMP observation of neutral density, the IMF clock angle, and the IMF y and z components. The IMF values are derived from ACE measurements by shifting a specified time forward according to the solar wind average speed during the event. The Joule heating rate and location in the simulation agree well with DMSP Poynting flux. The enhancement at ~07:50 UT agrees well on magnitude, timing, and duration.

[13] Using the magnetospheric magnetic field in the simulation and the Earth's dipole field in the ionosphere, we trace the magnetic field lines from locations at and near the DMSP location at 07:50 UT when the DMSP observes the large enhancement of Poynting flux. These field lines are found to be open, as shown by the cyan lines in Figure 2 that overdrape the northern dawn flank of the magnetopause.

[14] To find out how these open field lines are formed, we trace a fluid element on one of the open field lines backward in time and compute the magnetic field line threading through the fluid element for each integrating step. Figure 3 shows some of resulting magnetic field lines in cyan and the path of the fluid element in blue. The total traverse time of

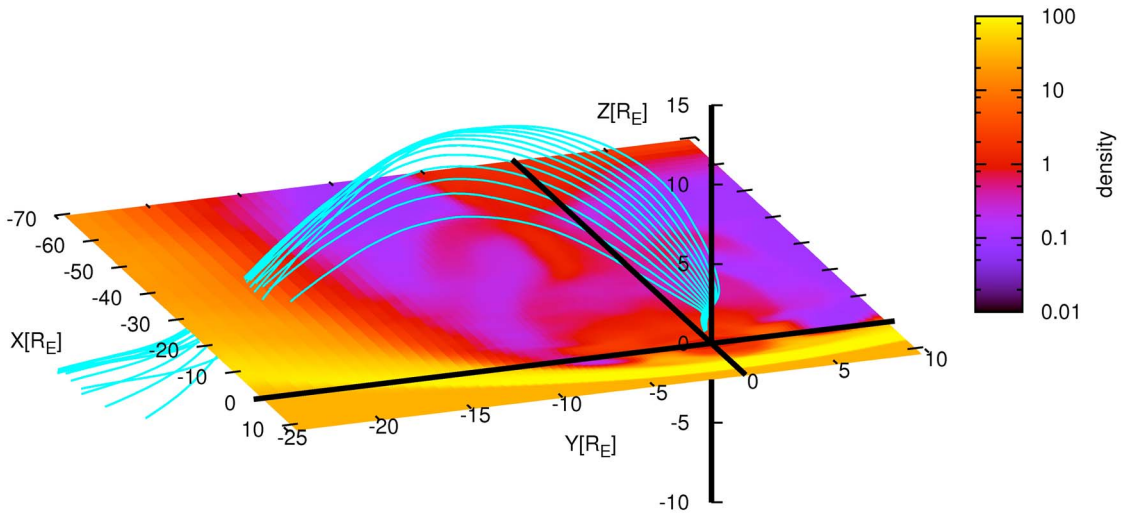

Figure 2. A 3-D view of the magnetic field lines that are traced from the DMSP F15 location at 07:50:00 UT on 24 August 2005 and its nearby points. The GSE equatorial plane shows the color-coded density (cm^{-3}) for the same time.

the plasma element on this path is 20 min. Counting from the Sun along the path shown in Figure 3, the first three field lines are IMF field lines. The fourth field line is an open field line with a sharp kinked section indicating that it is a result of the reconnection between the IMF and the cusp field near the nightside dusk flank [e.g., *Dungey*, 1963; *Cowley*, 1983; *Onsager et al.*, 2001; *Phan et al.*, 2003; *Lavraud et al.*, 2005; *Li et al.*, 2008]. This newly created open field line is then convected along the magnetopause toward the nightside, as shown by the following open field lines along the path. The foot point of this open field line moves from the dusk region to a place near the noon sector as indicated by the crosses in Figure 4. It should be noted that the field lines in Figure 2 are on the same time (07:50 UT) while the field lines in Figure 3 and their foot point motions in Figure 4 are on different times due to the traverse of a fluid element.

[15] Figure 5 shows the distributions of Joule heating rate and FAC in the northern polar region at 07:50 UT. Red indicates the strong Joule heating rate region. The thick red line and the arrowhead indicate that the DMSP F15 satellite was passing through this region around 07:50 UT. The

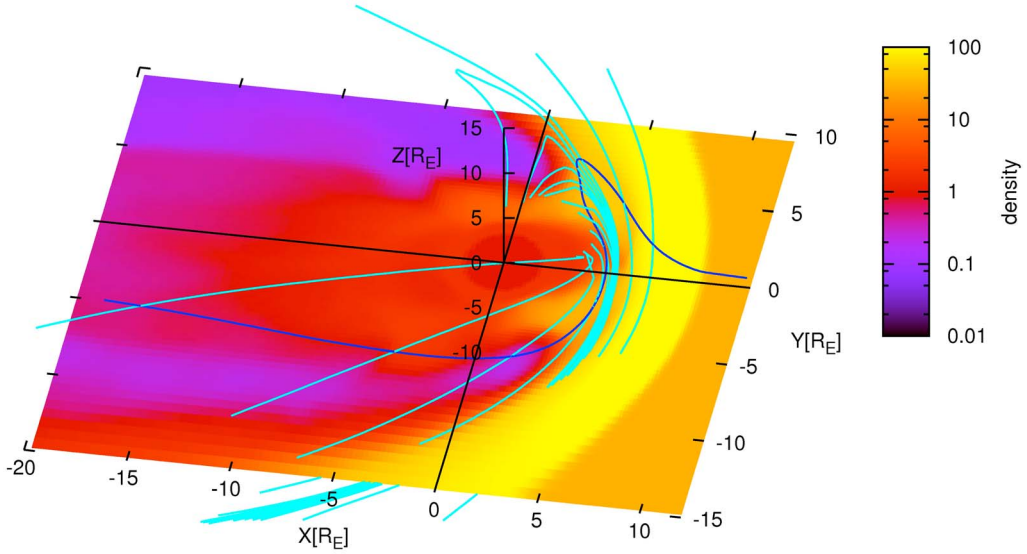

Figure 3. A 3-D view, from slightly above the dawnside cusp, of the path (blue) of a fluid element and the magnetic field lines (cyan) that are attached to this fluid element. The fluid element moves from (21.0, −0.4, 1.2)R_E near the GSE X axis upward along the magnetopause to (2.7, 4.0, 5.4)R_E, turns around, moves downward and westward along the magnetopause, passes through the X = 0 plane at (0.0, −9.9, 6.3)R_E, and then reaches (−16.8, −11.8, 12.0)R_E, which is the end point of the shown section of this path. This fluid element takes 20 min to traverse this section of path. The GSE equatorial plane shows the color-coded density (cm^{-3}) at 07:50:00 UT on 24 August 2005.

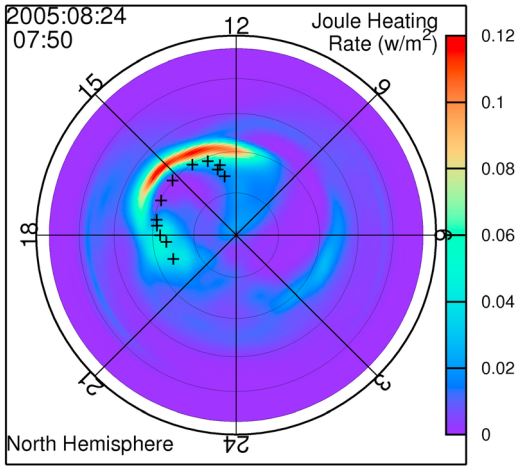

Figure 4. The ionospheric foot points of the open field lines shown in Figure 3. The crosses are the foot points. The background is the distribution of the OpenGGCM Joule heating rate in the ionosphere in the Northern Hemisphere at 07:50:00 UT on 24 August 2005. The thin latitude circles are 10° away from each other in SM coordinates.

enhanced Joule heating region is located between two adjacent and opposite high-latitude strong FACs. As shown in Figure 1, the IMF clock angle near the magnetopause is about 75° around 07:50 UT with a 20.5 nT IMF B_y and a 5.1 nT IMF B_z.

[16] The pair of adjacent and opposite FACs shown in Figure 5 looks similar to the iridium FAC distribution for duskward IMF shown in Figure 1d of *Anderson et al.* [2008]. Note that the positive (red) FAC is downward in Figures 1–19. From iridium data, *Anderson et al.* [2008] computes the average FAC distributions for various IMF directions as well as the associated **E** × **B** flow channel. The FAC distribution in Figure 5 obviously has some differences compared to that in Figure 5 (NE) of *Anderson et al.* [2008] because the latter is a statistical average value for medium clock angle (~45°). However, they share a common feature: a pair of adjacent and opposite FACs with the upward FAC locating poleward of the downward one. The **E** × **B** flow channel in Figure 5 (NE) of *Anderson et al.* [2008] is consistent with the primarily sunward motion of the open field line shown in Figures 3 and 4. Both the **E** × **B** flow channel and the narrow latitudinal hot Joule heating region exist in between the opposite FACs. A Northern Hemisphere sunward **E** × **B** flow channel between a downward and upward FAC pair for northward IMF conditions has also been reported by *Eriksson et al.* [2008] from DMSP observations.

[17] The slab model [*Cravens*, 1997; *Tanaka*, 2007] shown in Figure 6 explains how the FACs, the ionospheric currents, and the Joule heating hot spots are formed. One can either assume a mechanical viewpoint that focuses on the magnetic field and plasma motion (**B**, **V**) or an electrodynamic viewpoint that emphasizes the electric field and currents (**E**, **J**) [*Parker*, 1996]. In the mechanical view, reconnection creates open field lines. At high latitudes, the open field lines are dragged by the solar wind tailward for southward IMF. For northward IMF, the open field lines are first dragged sunward then around the flanks tailward, as shown in Figure 3. The magnetic field transmits these stresses to the ionosphere, where the field lines, along with the ionospheric plasma, move through the background neutrals. Collisional friction between the neutrals and the ions then cause the heating [*Strangeway and Raeder*, 2001]. In the electrodynamic view, reconnection causes shear of the magnetic field between the reconnected field lines and the surrounding field. Such a shear corresponds to field-aligned currents, and thus there is a pair of FAC sheets between the reconnection region and the ionosphere. Current continuity ($\nabla \cdot \mathbf{J} = 0$) demands that these currents close both in the reconnection region and in the ionosphere. In the reconnection region, $\mathbf{E} \cdot \mathbf{J} = \mathbf{V} \cdot (\mathbf{J} \times \mathbf{B})$ is negative; thus, it is a dynamo region. In the ionosphere, resistivity dominates; thus, $\mathbf{E} \cdot \mathbf{J} \sim \sigma E^2 > 0$ and the electromagnetic energy is

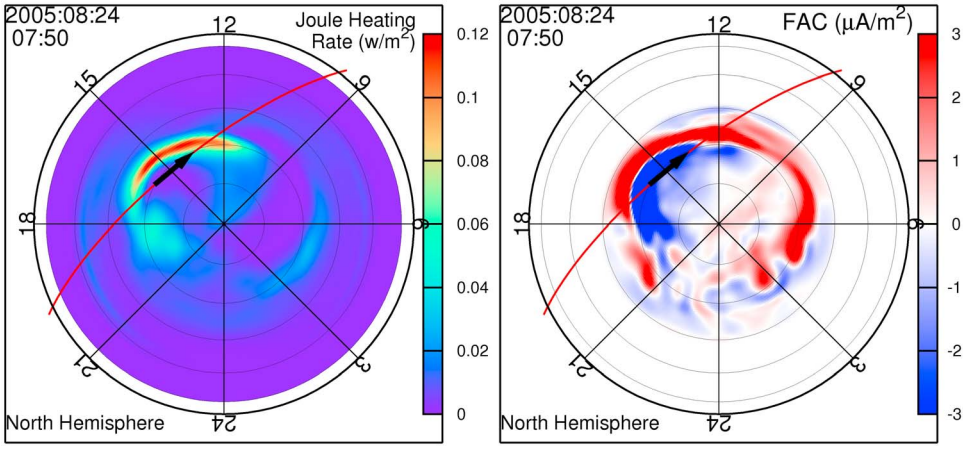

Figure 5. The distribution of the OpenGGCM Joule heating rate (left) and FAC (right) in the ionosphere in the Northern Hemisphere at 07:50:00 UT on 24 August 2005. The thin latitude circles are 10° away from each other in SM coordinates. Positive FAC is downward. The thick red line represents the track of DMSP F15, whose location at 07:50:00 UT on 24 August 2005 is indicated by the arrowhead.

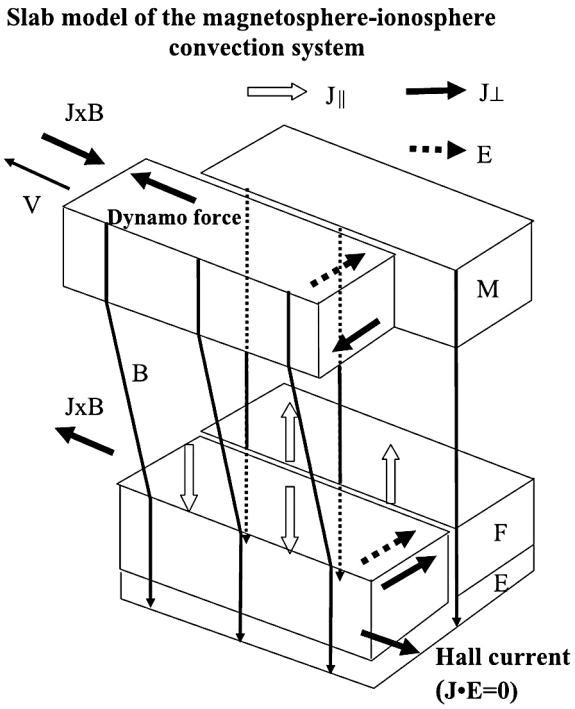

Figure 6. Slab model of the convection. M, F, and E represent the magnetospheric (or magnetosheath) domain, the ionospheric F layer, and the ionospheric E layer, respectively. The entire system is coupled by a magnetic field (solid lines with downward arrows). Figure 6 represents a moment at which shear motion is generated in the M region and the front portion is just beginning to move. In this moment, FAC (white arrows), ionospheric current (solid arrows), and magnetospheric current (solid arrows) form a closed circuit. **E** and **J** are antiparallel ($\mathbf{J} \cdot \mathbf{E} < 0$) in the magnetosphere, while they are parallel in the ionosphere ($\mathbf{J} \cdot \mathbf{E} > 0$). Reprinted from *Tanaka* [2007, Figure 2] with kind permission of Springer Science and Business Media.

dissipated here. Although the mechanical view is more fundamental, **E** and **J** are easier to observe and to analyze.

[18] For the example shown in Figure 5, the solar wind dynamo force, possibly in combination with the $\mathbf{J} \times \mathbf{B}$ force near the kinked section of an open field line, drives the foot section of the open flux tube sunward from the dusk region toward noon (Figure 4). The results are a latitudinal $\mathbf{E} \times \mathbf{B}$ flow channel, a poleward perpendicular Pedersen current, and a pair of the downward and upward FACs that flank this Pedersen current and connect to the magnetospheric current to form a closed circuit. This Pedersen current then creates a Joule heating region. Therefore, a stronger FAC means a stronger ionospheric current and thus a higher Joule heating rate ($\mathbf{J} \cdot \mathbf{E}$) and a more intense downward Poynting flux in the ionosphere.

[19] Referring back to Figure 1, DMSP F15 observes a high level of Poynting flux at ~07:50 UT in the Northern Hemisphere but does not observe significant Poynting flux when passing through the southern polar region at ~07:00 UT nor through the northern polar region at ~06:05 UT. It is likely that the spacecraft does not pass through the region with a high level of local Poynting flux. Figure 7 shows that the level of the Joule heating rate in a narrow arc in the northern polar region is ~40 mW m^{-2} at ~06:05 UT when the IMF clock angle is about 30°. Both the IMF y and z components are modest, about 5 and 8 nT, respectively. The Joule heating region indicated by cyan in Figure 7 is located in the afternoon region when the IMF y component is positive, and the cusp reconnection occurs at the duskside of the cusp. This narrow region is between a pair of adjacent and opposite FACs. Although the observed DMSP Poynting flux is almost zero, the OpenGGCM Joule heating rate is significant. The arrowhead in Figure 7 indicates that the DMSP F15 is on the edge of the narrow arc of the Joule heating region at ~06:05 UT. This slight discrepancy may be caused by the Earth's dipole setting in the simulation. OpenGGCM uses a fixed dipole which is set for 12:00:00 UT on 24 August 2005 in this event simulation. It is most likely that DMSP F15 actually does not fly through the hot spot during this polar pass but the hot spot still exists.

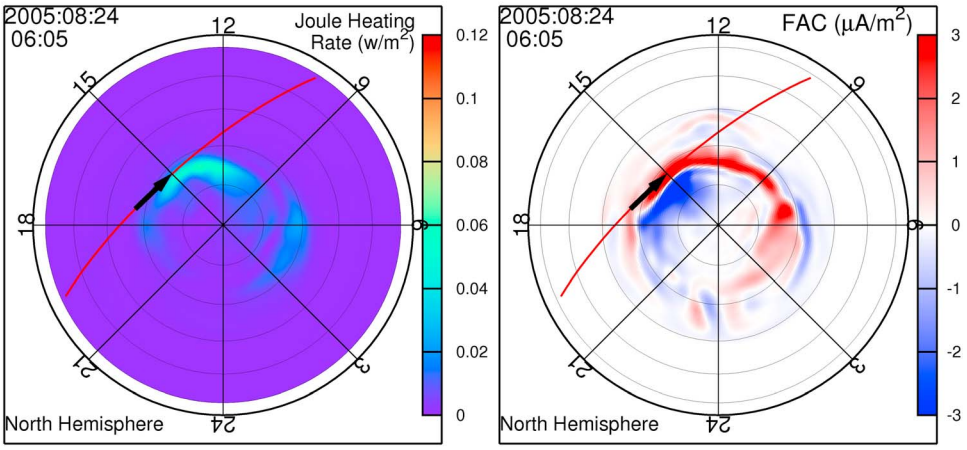

Figure 7. Same as Figure 5 but for the Northern Hemisphere at 06:05:00 UT on 24 August 2005. Positive FAC is downward.

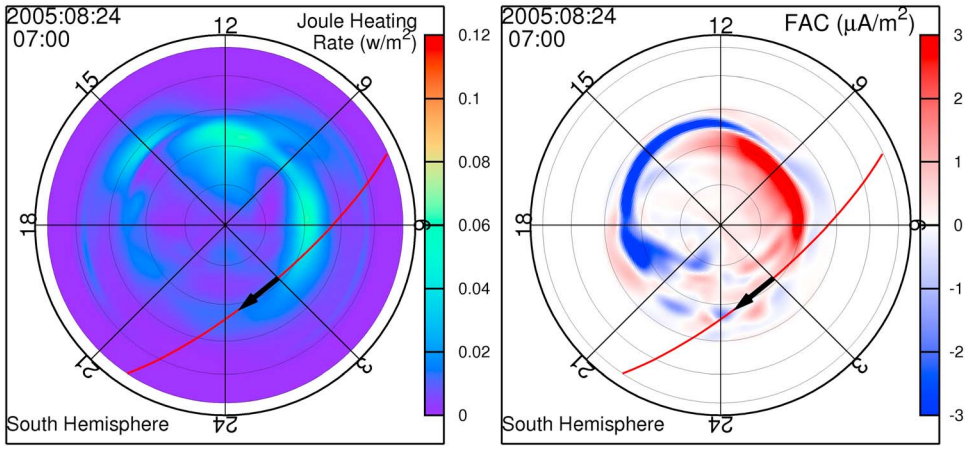

Figure 8. Same as Figure 5 but for the Southern Hemisphere at 07:00:00 UT on 24 August 2005. Positive FAC is downward.

[20] The Southern Hemisphere distributions of the Joule heating rate and FAC at ~07:00 UT shown in Figure 8 are significantly different from those in the Northern Hemisphere for ~06:05 and ~07:50 UT. Around ~07:00 UT, the IMF is almost in the ecliptic plane and is slightly southward for a brief period. The IMF y component is large with a value of 16 nT, and the IMF z component is very small. In the Southern Hemisphere, Joule heating hot spots and regions of strong FAC are all missed by the DMSP F15 spacecraft during the pass around 7:00 UT.

[21] During this event, the CHAMP satellite observed high neutral density increases in both polar regions at ~07:00 and ~07:35 UT, as shown in Figure 1. CHAMP did not observe the density enhancement during previous polar passages for the time period from 04:00 to 06:00 UT, during which both the IMF clock angle and magnitude were small before becoming large after ~06:00 UT. Therefore, the density enhancements are likely caused by the Joule heating dissipated by open field lines as a result of cusp reconnection for northward IMF with a large clock angle and large y component. The enhancements thus are closely connected to the enhanced Poynting flux observed by DMSP F15 as suggested by *Crowley et al.* [2010]. However, how the Joule heating enhancement associated with the cusp reconnection affects the thermosphere needs further observation and simulation studies and is not the topic of this paper.

4. Event 7 November 2004

[22] Figure 9 shows the DMSP F15 observation of Poynting flux, the corresponding Joule heating rate in the simulation, the DMSP latitude and longitude in SM coordinates, the IMF clock angle, and the IMF y and z components for 7 November 2004 from 18:00 to 20:00 UT. The Joule heating rate in the simulation agrees well with DMSP Poynting flux, especially for the enhancement at ~19:05 UT, which agrees on magnitude, timing, and duration.

[23] During this event, the DMSP F15 observes a high level of Poynting flux in the Southern Hemisphere at ~19:05 UT (IMF clock angle ~45°, B_y ~28 nT) but does not observe significant Poynting flux when passing through the northern polar region at ~18:21 UT (IMF clock angle ~18°, B_y ~6 nT) and at ~19:54 UT (IMF clock angle ~31°, B_y ~23 nT).

[24] Figure 10 is similar to Figure 5 but shows a high Joule heating rate region in the southern polar region morning sector because the cusp reconnection occurs at the dawnside of the southern cusp and at the duskside of the northern cusp when the IMF is northward with a positive y component. Clearly, the Joule heating hot spot is located between two adjacent and opposite strong FACs with the downward (positive) one being poleward of the upward (negative) one in contrast to the Northern Hemisphere event at 7:50 UT, discussed in section 3. In this case, with the upward magnetic field near the southern polar region, the foot points of the open field lines move eastward from the dawn region and cause an equatorward Pedersen current; hence the corresponding pair of FACs. The DMSP F15 spacecraft crosses the hot spot of Joule heating at ~19:05 UT.

[25] At ~18:21 UT, there are regions of enhanced Joule heating and FACs in the afternoon sector of the northern polar region, as shown in Figure 11. In comparison to the hot regions in Figure 10, these hot regions are smaller and less intense and are missed by the DMSP F15 spacecraft. Around ~18:21 UT, the IMF is strong (B_z ~20 nT) but has a small clock angle (~18°). A small clock angle will lead to a short distance of movement of a foot point of an open field line and therefore a small spot of Joule heating (more discussion in section 6).

[26] From ~19:40 to ~19:51 UT, the IMF B_y is negative. It means that the cusp reconnection occurs in the dawnside of the northern cusp and creates open field lines whose foot points move eastward, thus generating the equatorward Pedersen current and a downward FAC located poleward of a upward FAC in the Northern Hemisphere. This pair of FACs in Figure 12 agrees well with that shown by Figure 5 (NW) of *Anderson et al.* [2008]. Around ~19:54 UT, the IMF rotates rapidly from a clock angle ~−45° to ~45° within 5 min while keeping the northward direction. Around this time, the DMSP F15 spacecraft in the premidnight sector observes little Poynting flux. The Joule heating rate along the spacecraft trajectory in the simulation is also very low except for a small hot spot located near 09:00 MLT. Although

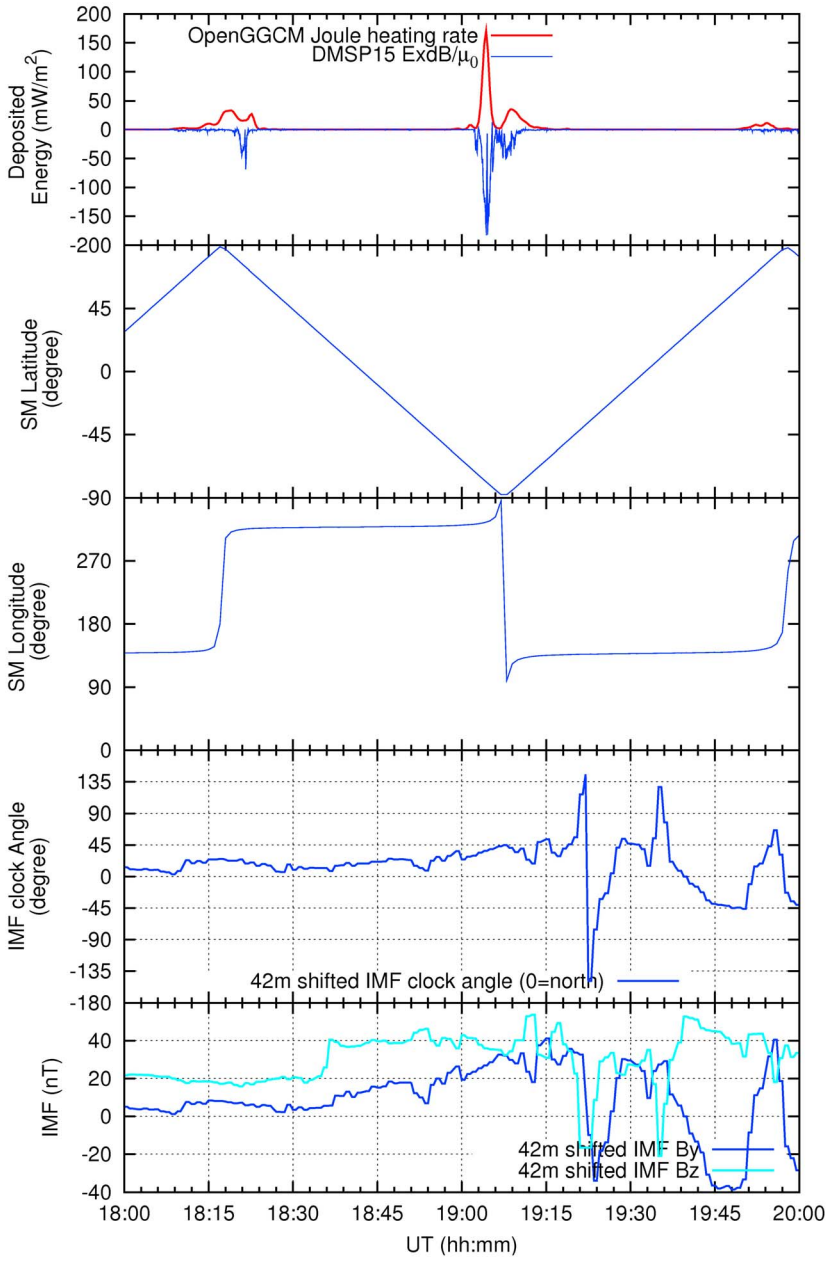

Figure 9. Observation and simulation results for 7 November 2004. From top to bottom are DMSP F15 observation of Poynting flux and the corresponding Joule heating rate on the virtual DMSP orbit in the simulation, DMSP latitude in SM coordinates, DMSP longitude in SM coordinates, the one-AU IMF clock angle derived from ACE measurement, and the one-AU IMF y and z components derived from ACE data.

there is a Joule heating hot spot on the track ahead of the spacecraft for the 19:54 UT simulation step (Figure 12), it disappears when the spacecraft passes the location of this spot at ~20:00 UT (Figure 13).

5. Event 21 January 2005

[27] Figure 14 shows the same parameters as in Figure 9 for the time period from 17:00 to 21:00 UT on 21 January 2005. During this event, the DMSP F15 spacecraft observes an enhancement of Poynting flux at ~20:00 UT and a low level of Poynting flux for other polar passes. The OpenGGCM Joule heating along the spacecraft track agrees well with this observation of Poynting flux.

[28] For the northern polar pass around 17:36 UT, the IMF is southward and the modest Joule heating area is near noon, as indicated by Figure 15. The Joule heating hot spot is still flanked by two opposite FACs. Here the positive IMF y component and the flow channel in Figure 5 (SE) of *Anderson et al.* [2008] suggest that the foot points of the open field lines created by a subsolar magnetopause reconnection move westward from noon, therefore creating

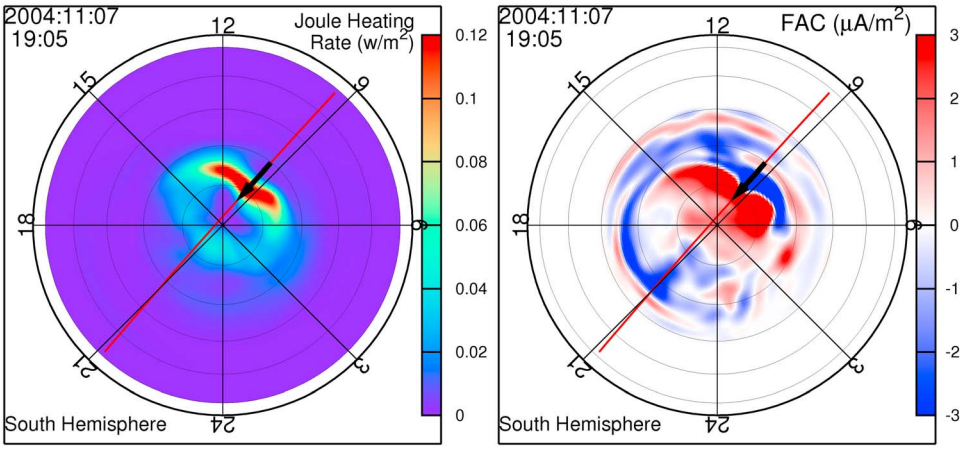

Figure 10. Same as Figure 5 but for the Southern Hemisphere at 19:05:00 UT on 7 November 2004. Positive FAC is downward.

the Joule heating region from noon to the prenoon sector and the corresponding pair of FACs. Indeed, the distribution of FACs shown in Figure 15 is basically consistent with that shown in Figure 5 (SE) of *Anderson et al.* [2008]. The large FACs shown in Figures 5 and 10 are absent. The DMSP F15 spacecraft does not sample the heating region for this polar pass.

[29] For the southern polar pass around 18:30 UT, the IMF is also southward but rapidly rotates toward a pure southward direction. Figure 16 shows a low-intensity Joule heating spot near the noon sector. The Joule heating hot spot at noon is flanked by a pair of opposite FACs. The DMSP F15 spacecraft does not pass through this hot region but instead through a broad, less intense Joule heating region in the nightside, which may result from reconnection in the tail. The spacecraft thus observed a rather modest Poynting flux (average ~25 mW m^{-2}) around 18:30 UT.

[30] For the polar pass around 19:24 UT, the IMF is basically dawn-dusk and slightly southward. Figure 17 shows a hot area near the noon region and several scattered weaker Joule heating areas. The FAC distribution is consistent with that shown in Figure 1d of *Anderson et al.* [2008]. The DMSP F15 spacecraft also does not pass through the hot region but was barely on the edge that allows the observation of a Poynting flux of 50 mW m^{-2} around 19:24 UT.

[31] Figure 18 shows that a large, enhanced Joule heating area covers the prenoon region at ~20:00 UT. The DMSP F15 spacecraft just passes the edge of this area and thus observes a strong downward Poynting flux. This Joule heating hot spot is also flanked by a strong downward (positive) FAC at its poleward side and a strong upward (negative) FAC at its equatorward side. The distribution is similar to that shown in Figure 10. The IMF has a large clock angle (~65°) and a large y component (~15 nT). Figure 19 shows the field lines traced from the Southern Hemisphere ionospheric locations (shown in Figure 18) near the DMSP F15 spacecraft at 20:00 UT. These open field lines suggest that cusp reconnection is occurring near the southern dawnside flank of the cusp at ~20:00 UT. Their foot points indicate that the open field lines move toward noon from the morning region. It should be noted that the

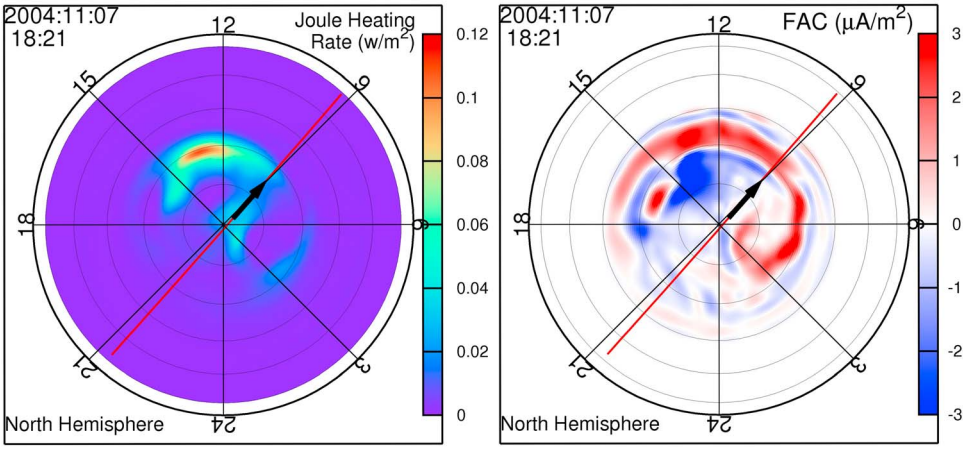

Figure 11. Same as Figure 5 but for the Northern Hemisphere at 18:21:00 UT on 7 November 2004. Positive FAC is downward.

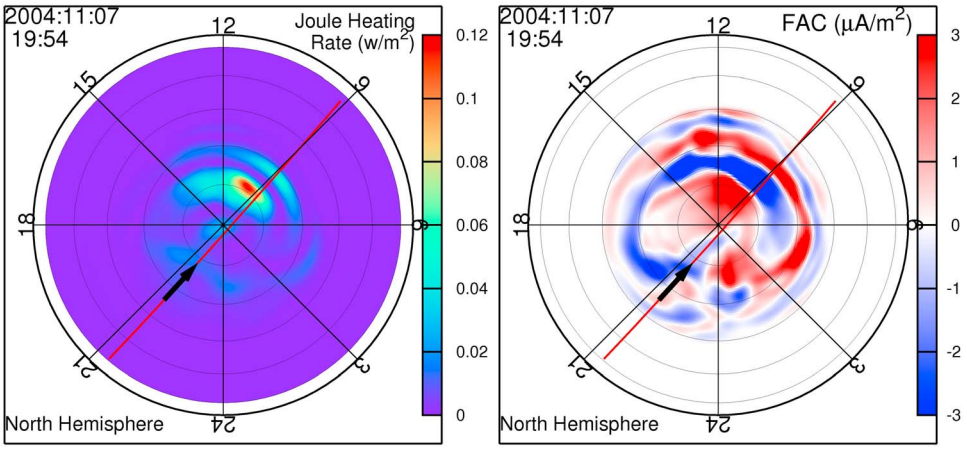

Figure 12. Same as Figure 5 but for the Northern Hemisphere at 19:54:00 UT on 7 November 2004. Positive FAC is downward.

field lines in Figure 19 are on the same time (20:00 UT) while the field lines in Figure 3 are on different times due to the traverse of a fluid element.

6. Discussion

[32] We have studied the Poynting flux observed by DMSP F15 spacecraft and the corresponding distributions of the Joule heating rate and FAC in OpenGGCM simulations for three events. During these three events, the DMSP F15 spacecraft observes strong enhancements of Poynting flux in the dayside high-latitude region. Our OpenGGCM simulations for these events reproduce the ionospheric Joule heating and agree very well with the observed Poynting flux. This result is expected because the Poynting flux into the ionosphere should be equal to the energy dissipated by the Joule heating under time-stationary conditions and the assumption that no energy goes into accelerating the plasma.

[33] The downward Poynting flux observed by DMSP F15 spacecraft during periods of northward IMF with large y component can be up to 180 mW m^{-2}, which is extremely large compared to maximum values on the level of a few tens mW m^{-2} that have been observed during moderate storms and significantly larger than the 110 mW m^{-2} reported during a very large substorm of the 6 April 2000 superstorm [*Huang and Burke*, 2004]. However, it is still possible that previous and current satellites have simply missed the local time with extremely high Poynting flux during substorms or storms. In this paper, we show that such extreme Poynting flux is caused by high-latitude reconnection under conditions of large IMF clock angle and large IMF magnitude.

[34] The simulation results show that there is a latitudinal region of high Joule heating rate in the dayside high-latitude region between ~60° (~−60°) SM and ~80° (~−80°) SM latitude in the Northern (Southern) Hemisphere for northward IMF conditions. This region extends from noon to dawn (dusk) for the positive (negative) IMF y component in the Northern Hemisphere and extends to an opposite direction in the Southern Hemisphere. A larger IMF clock angle leads to a larger area of Joule heating, which may span 60°–

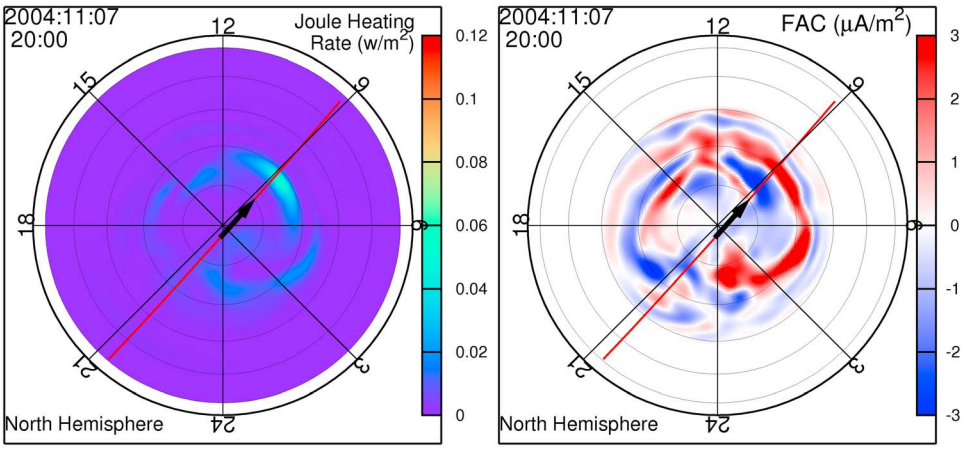

Figure 13. Same as Figure 5 but for the Northern Hemisphere at 20:00:00 UT on 7 November 2004. Positive FAC is downward.

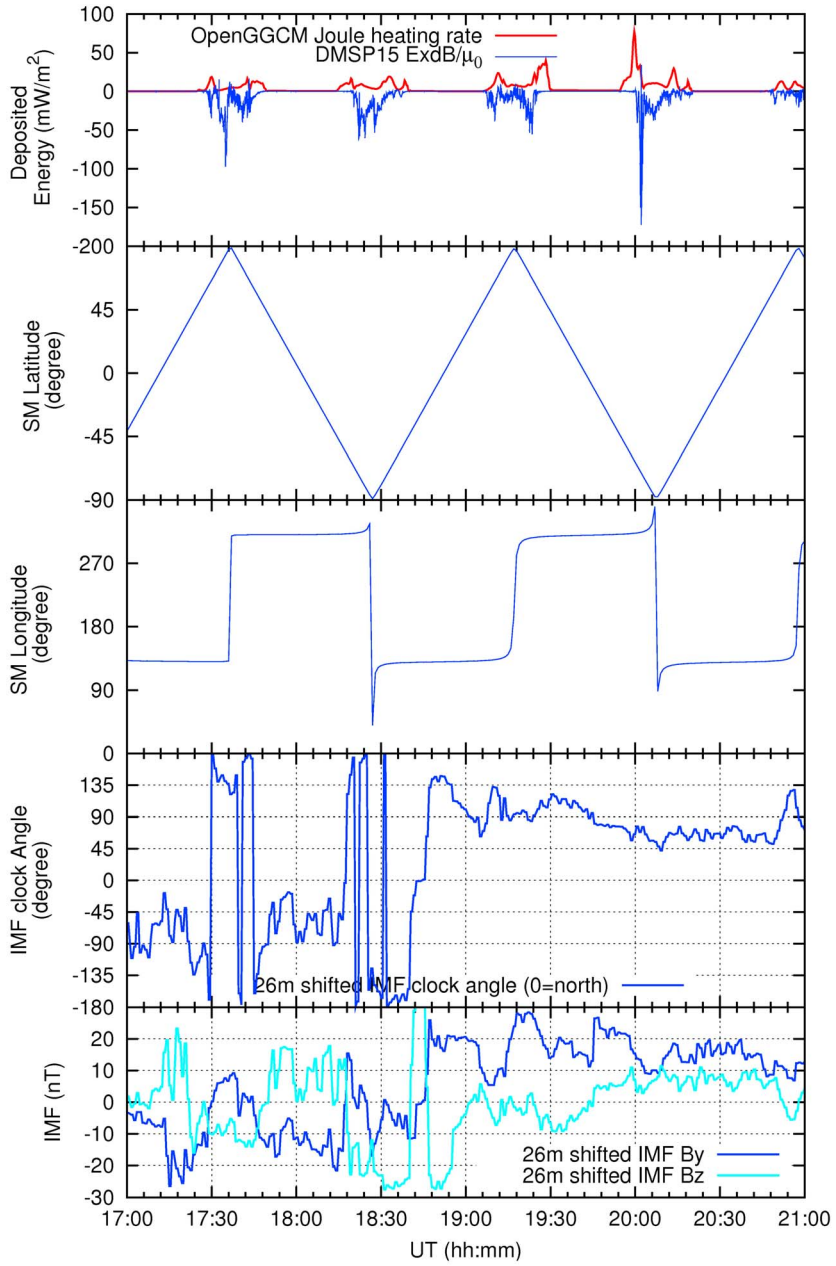

Figure 14. Observation and simulation results for 21 January 2005. From top to bottom are DMSP F15 observation of Poynting flux and the corresponding Joule heating rate on the virtual DMSP orbit in the simulation, DMSP latitude in SM coordinates, DMSP longitude in SM coordinates, the one-AU IMF clock angle derived from ACE measurement, and the one-AU IMF y and z components derived from ACE data.

100° in longitude and 5°–10° in latitude. The maximum value of the Joule heating rate can be as high as 100–200 mW m^{-2}. The extremely strong Poynting flux cases (Figures 5, 10, and 18) shown in this paper are all associated with large IMF clock angle (75°, 45°, and 65°, respectively), very strong IMF (22.6, 46.4, and 25.7 nT, respectively), and moderate to high dynamic pressure (7.4, 16.6, and 24.9 nPa, respectively). It seems that the intensities of the dayside Joule heating and the downward Poynting flux are likely closely related to IMF magnitude and solar wind dynamic pressure.

[35] The heated region is always flanked by two adjacent and opposite high-latitude FAC sheets, where the downward FAC locates equatorward (poleward) of the upward FAC at the afternoon (morning) sector, respectively, for both Northern and Southern hemispheres. The scale and magnitude of such FACs seem to be proportional to the scale and magnitude of the Joule heating rate.

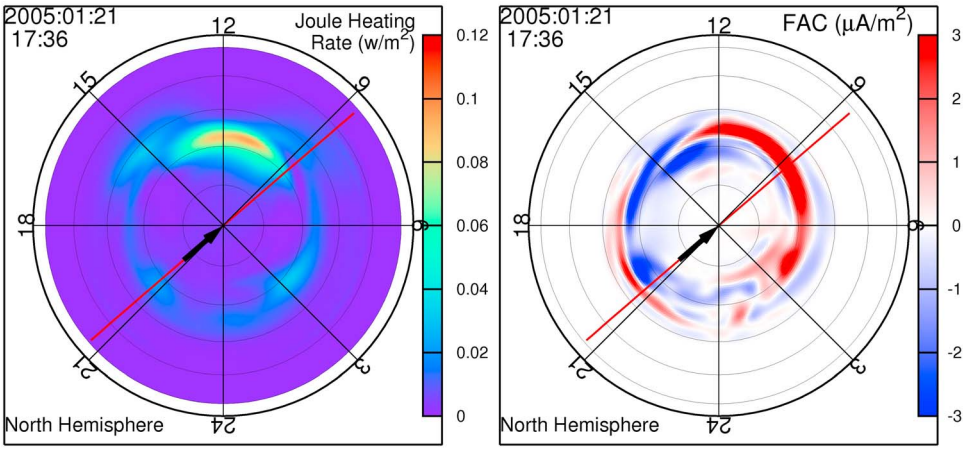

Figure 15. Same as Figure 5 but for the Northern Hemisphere at 17:36:00 UT on 21 January 2005. Positive FAC is downward.

[36] The characteristic distributions of the Joule heating and the corresponding FACs are more likely observed by DMSP F15 for IMF conditions with a large clock angle (>~45°) and a large *y* component (>~10 nT) because the spacecraft orbit is near the 09:00–21:00 LT meridian. For IMF conditions with a small clock angle, the spacecraft will more likely miss the region of strong Poynting flux.

[37] As suggested by the slab model (Figure 6), magnetic field lines moving in the conducting ionosphere create Pedersen current, its associated Joule heating, and its associated FACs. Therefore, the distributions of the Joule heating rate and the corresponding FACs are directly related to the movement of field lines, which is closely related to reconnection and solar wind dynamo. Their intensities are closely related to IMF magnitude and solar wind dynamic pressure because the creation of Joule heating and Poynting flux is mainly a result of the movement of open field lines, which are mainly a part of the solar wind and IMF.

[38] There are two reasons why a larger IMF clock angle tends to lead to a larger area of intense Joule heating. One is related to the position of the reconnection site and the way in which a newly created open field line drapes around the magnetopause [*Li et al.*, 2008]. When the IMF clock angle is large, the reconnection site tends to be near the flank, a newly created open field line tends to have a foot point further away from the midnight-noon meridian, and an open field line with duskside (dawnside) foot point tends to drape mainly westward (eastward), respectively, around dayside magnetopause toward the tail, as shown in Figures 3 and 19. This draping behavior causes the foot section of the open field line to move latitudinally from duskside or dawnside to the noon region, as indicated in Figure 4, leading to an extended latitudinal Joule heating area in the dayside where conductance is high due to solar EUV irradiation. On the other hand, when IMF clock angle is small, the open field line mainly drapes northward or southward around the magnetopause, causing its foot section to move directly from poleward cusp to equatorward cusp and thus leading to a small region of Joule heating near the noon region as shown in Figures 7 and 11.

[39] The other reason is that the lifetime of an open field line resulting from cusp reconnection is longer for a larger IMF clock angle. Some open field lines may not become closed in the dayside and are just convected toward the tail.

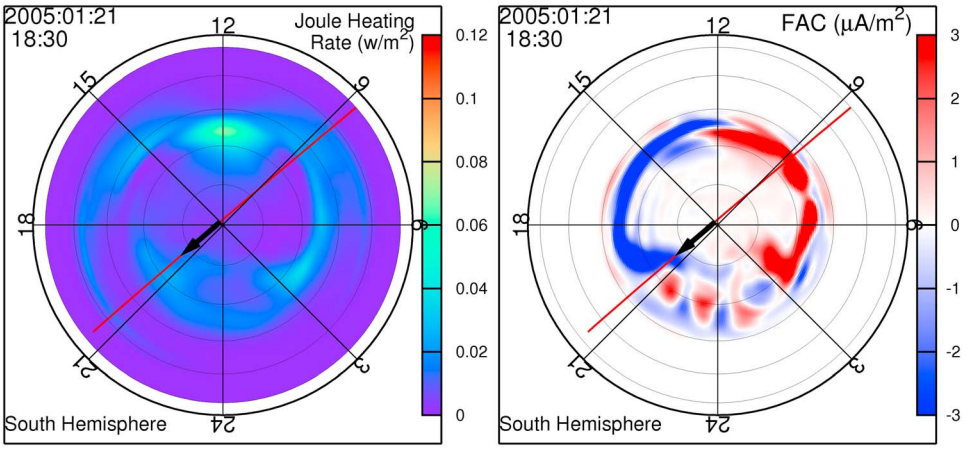

Figure 16. Same as Figure 5 but for the Southern Hemisphere at 18:30:00 UT on 21 January 2005. Positive FAC is downward.

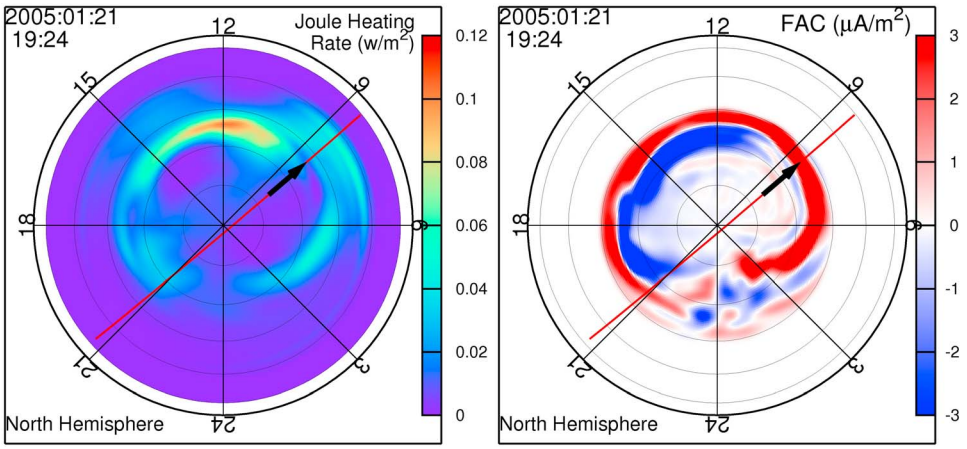

Figure 17. Same as Figure 5 but for the Northern Hemisphere at 19:24:00 UT on 21 January 2005. Positive FAC is downward.

When the IMF is northward and the clock angle is small, the open field line becomes closed shortly after it is created [*Li et al.*, 2005, 2008]. After becoming a closed field line, the solar wind dynamo force stops acting on the ionosphere through open field lines. Figure 4 of *Li et al.* [2005] is similar to Figure 3 except for its IMF with small clock angle. Both Figures 3 and 4 show the path of a fluid element from the solar wind and the corresponding field lines threading this element at different time steps. The field line in Figure 4 changes rapidly from IMF to open and then to closed, while it stays open for a rather long time in Figure 3. Figures 3 and 4 use the same integrating time step when computing the fluid element path. One can find more detailed information about the behaviors of the field lines involving cusp reconnection in the MHD study by *Li et al.* [2008] and references therein.

[40] While the field lines in the strong Joule heating region are usually open, we also found closed field lines there. When a closed field line is formed as a result of the reconnection on both cusps, both of its foot sections first move from poleward cusp toward equatorward cusp, resulting in a Joule heating region at the noon cusp region. This closed field line is then convected tailward along the flanks. Both of its foot sections thus move toward nightside along a latitudinal arc, creating Joule heating there. The Joule heating created by the movement of closed field lines is weaker than that created by moving open field lines because the solar wind dynamic force cannot directly act on the ionospheric foot sections of the closed field lines.

[41] The motion of the foot sections of the newly created open (or closed) field lines as a result of cusp reconnection agrees very well with the observed flow channels shown in Figure 5 of *Anderson et al.* [2008]. As suggested by the slab model shown in Figure 6, such motion determines the direction, scale, and magnitude of a Pedersen current and the neighboring FACs that connect to the outer magnetosphere to make a closed circuit. Since Pedersen current causes Joule heating and the currents flow in a closed circuit, the scale and magnitude of the Joule heating region is proportional to those of the FACs.

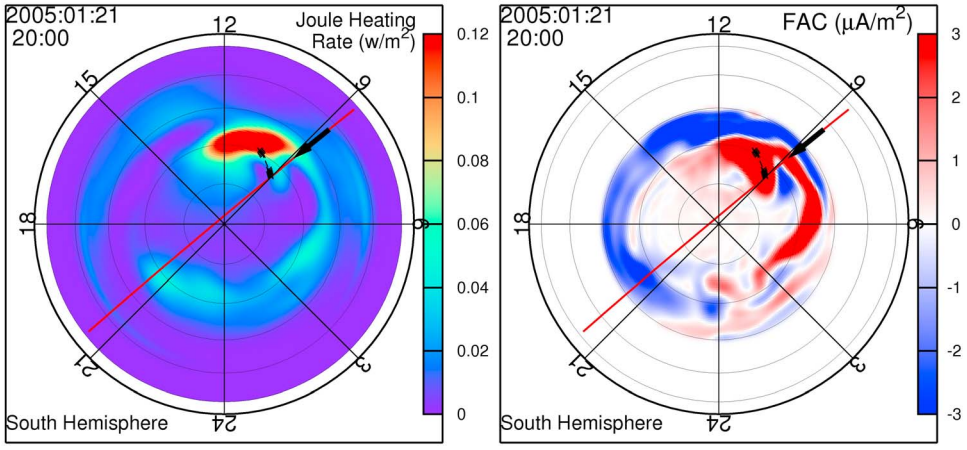

Figure 18. Same as Figure 5 but for the Southern Hemisphere at 20:00:00 UT on 21 January 2005. The two clusters of points near both the hot Joule heating spot and the DMSP are the foot points of the open field lines shown in Figure 19. The most westward point corresponds to the most dawnward open field line. The points are so close that they look like two points.

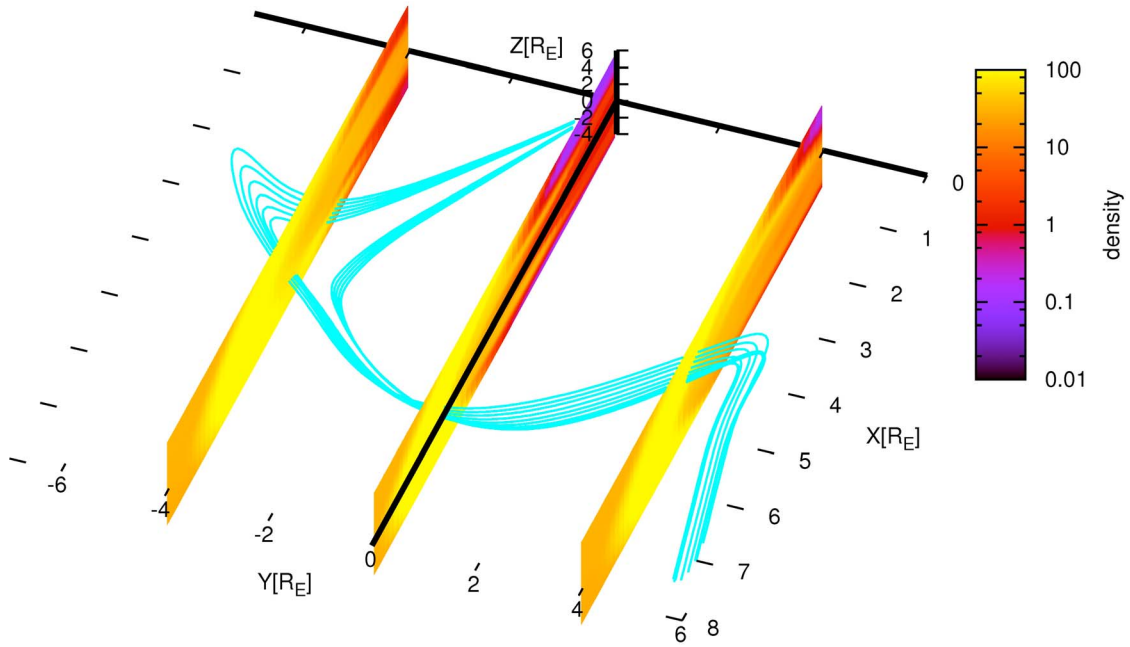

Figure 19. The magnetic field lines that are traced from points (shown in Figure 18) near the DMSP F15 location at 20:00:00 UT on 21 January 2005. The three color-coded density (cm^{-3}) planes are located at $y = -4$, $y = 0$, and $y = 4$.

[42] Once an open field line is created, solar wind ions and electrons will precipitate along the field line down to the ionosphere, resulting in cusp aurora. Intense proton aurora spots in the cusp region during northward IMF conditions have been observed by the Imager for Magnetopause-to-Aurora Global Explorations (IMAGE) Far Ultraviolet Instrument (FUV) [*Berchem et al.*, 2003; *Bobra et al.*, 2004]. Most of the observed locations of proton aurora coincide with the locations mapped to the antiparallel reconnection sites tailward of the cusp. They should also coincide with the **E** × **B** flow channels discussed in section 3. Both the location of the cusp proton aurora and the location of the flow channel are effectively controlled by IMF B_y. Since there is no sufficient IMAGE FUV data coverage for the events studied in this paper and there was a partial failure of the DMSP F15 ion detector, we cannot perform valuable comparisons here. A future study incorporating cusp aurora data will be needed to further confirm the cusp-related mechanism studied in this paper.

[43] When the IMF is southward, Joule heating occurs around noon and between ~60° (~−60°) and ~80° (~−80°) SM latitude in the Northern (Southern) Hemisphere, respectively, in the absence of substorms and storms. It appears that the region of enhanced Joule heating for southward IMF with a large y component (Figures 15 and 16) is smaller than that for a northward IMF with a large y component (Figures 5 and 18). Again, the motion of the foot sections of the newly created open field lines due to magnetopause reconnection determines the distribution of the Joule heating rate and the corresponding FACs. The Joule heating regions are also located in the dayside because ionospheric conductivity is high due to solar EUV irradiation. Almost all the Joule heating figures shown in this paper display significant Joule heating distribution at or near noon. This suggests that a spacecraft is more likely to observe a high level of dayside Poynting flux frequently for both northward and southward IMF conditions if its orbit is near the noon-midnight meridian.

[44] When the IMF B_z is slightly negative and B_y is large, the magnetic reconnection process and reconnection sites seem to be more complicated than those for large IMF B_z conditions because the component reconnection most likely plays a significant role [*Trattner et al.*, 2005, 2007]. The reconnection site may extend across the entire dayside from dawn to dusk [*Trattner et al.*, 2007]. The behavior of newly open field lines may then become more complicated, and thus the Joule heating and corresponding FAC regions may look different than those for IMF with relatively large B_z. Figures 8 and 17, which show a significant Joule heating rate at dawn in addition to the hot spot at noon, and the corresponding IMF conditions shown in Figures 1 and 14, respectively, seem to be an indication of such a situation.

7. Conclusions

[45] In this paper, we show that the movement of the open field lines resulting from cusp reconnection causes a Joule heating region and a pair of neighboring opposite FACs in the dayside ionosphere cusp region for northward IMF conditions. For the events discussed here, localized heating values are in excess of 100 mW m^{-2}. In this Joule heating region, the observed earthward Poynting flux is approximately equivalent to the height-integrated Joule heating rate in the simulation. The intensities of the Joule heating, the earthward Poynting flux, and the FACs are closely related to the IMF magnitude. Their locations are mainly controlled by the IMF clock angle. A large IMF clock angle will lead to an extended latitudinal Joule heating (earthward Poynting flux)

region ranging from dawnside or duskside of the ionosphere cusp region to the noon region, depending on the direction of IMF B_y.

[46] The main purpose of this paper is the investigation of the mechanism that creates strong downward Poynting flux for northward IMF conditions. We have shown that cusp reconnection is ultimately responsible for the Poynting flux. All of the events we present here occur during periods of moderate to high solar wind flow, suggesting that solar wind speed plays a role. Future efforts will focus on quantifying the effect of solar wind speed and dynamic pressure.

[47] **Acknowledgments.** We acknowledge ACE, WIND, and CDAWeb for the solar wind data. The work was supported by grant ATM-0639658 from the National Science Foundation GEM and by AFOSR MURI award FA9550-07-1-0565 through a subcontract to the University of Colorado. Computations were performed on the Zaphod Beowulf cluster, which was in part funded by the Major Research Instrumentation program of the National Science Foundation under grant ATM-0420905 and on Teragrid facilities. Delores Knipp was partially supported by a National Research Council fellowship. The National Center for Atmospheric Research is sponsored by the National Science Foundation.

[48] Robert Lysak thanks the reviewers for their assistance in evaluating this paper.

References

Anderson, B. J., H. Korth, C. L. Waters, D. L. Green, and P. Stauning (2008), Statistical Birkeland current distributions from magnetic field observations by the iridium constellation, *Ann. Geophys.*, 671–687.

Berchem, J., S. A. Fuselier, S. Petrinec, H. U. Frey, and J. L. Burch (2003), Dayside proton aurora: Comparisons between global MHD simulations and IMAGE observations, *Space Sci. Rev.*, *109*, 313–349.

Bobra, M. G., S. M. Petrinec, S. A. Fuselier, E. S. Claflin, and H. E. Spence (2004), On the solar wind control of cusp aurora during northward IMF, *Geophys. Res. Lett.*, *31*, L04805, doi:10.1029/2003GL018417.

Cowley, S. W. H. (1983), Interpretation of observed relations between solar wind characteristics and effects at ionospheric altitudes, in *High Latitude Space Plasma Physics*, edited by B. Hultquist and T. Hagfors, pp. 225–249, Plenum, New York.

Cravens, T. E. (1997), *Physics of Solar System Plasmas*, 477 pp., Cambridge Univ. Press, Cambridge, U. K.

Crowley, G., D. J. Knipp, K. A. Drake, J. Lei, E. Sutton, and H. Luhr (2010), Thermospheric density enhancements in the dayside cusp region during strong B_y conditions, *Geophys. Res. Lett.*, *37*, L07110, doi:10.1029/2009GL042143.

Deng, Y., A. Maute, A. D. Richmond, and R. G. Roble (2008), Analysis of thermospheric response to magnetospheric inputs, *J. Geophys. Res.*, *113*, A04301, doi:10.1029/2007JA012840.

Dungey, J. W. (1963), The structure of the exosphere or adventures in velocity space, in *Geophysics, The Earth's Environment*, edited by C. DeWitt, J. Hieblot, and A. Lebeau, pp. 505–550, Gordon and Breach, Newark, N. J.

Eriksson, S., M. R. Hairston, F. J. Rich, H. Korth, Y. Zhang, and B. J. Anderson (2008), High-latitude ionosphere convection and Birkeland current response for the 15 May 2005 magnetic storm recovery phase, *J. Geophys. Res.*, *113*, A00A08, doi:10.1029/2008JA013139.

Foster, J. C., J. M. Holt, R. G. Musgrove, and D. S. Evans (1986), Solar wind dependencies of high-latitude convection and precipitation, in *Solar Wind-Magnetosphere Coupling*, edited by Y. Kamide and J. A. Slavin, pp. 477–494, Terra Sci., Tokyo.

Fuller-Rowell, T. J., D. Rees, S. Quegan, R. J. Moffett, M. V. Codrescu, and G. H. Millward (1996), A coupled thermosphere-ionosphere model (CTIM), in *STEP Report*, edited by R. W. Schunk, p. 217, Sci. Comm. on Sol. Terr. Phys., Boulder, Colo.

Gary, J., R. Heelis, W. Hanson, and J. Slavin (1994), Field-aligned Poynting flux observations in the high-latitude ionosphere, *J. Geophys. Res.*, *99*(A6), 11,417–11427, doi:10.1029/93JA03167.

Heelis, R. A., J. K. Lowell, and R. W. Spiro (1982), A model of the high-latitude ionospheric convection pattern, *J. Geophys. Res.*, *87*(A8), 6339–6345, doi:10.1029/JA087iA08p06339.

Heppner, J. P. (1972), Polar-cap electric field distributions related to the interplanetary magnetic field direction, *J. Geophys. Res.*, *77*(25), 4877–4887, doi:10.1029/JA077i025p04877.

Heppner, J. P., and N. C. Maynard (1987), Empirical high-latitude electric field models, *J. Geophys. Res.*, *92*(A5), 4467–4489, doi:1029/JA092iA05p04467.

Huang, C. Y., and W. J. Burke (2004), Transient sheets of field-aligned current observed by DMSP during the main phase of a magnetic superstorm, *J. Geophys. Res.*, *109*, A06303, doi:10.1029/2003JA010067.

Kelley, M. C., D. J. Knudsen, and J. F. Vickrey (1991), Poynting flux measurements on a satellite: A diagnostic tool for space research, *J. Geophys. Res.*, *96*(A1), 201–207, doi:10.1029/90JA01837.

Knipp, D., S. Eriksson, L. Kilcommons, G. Crowley, J. Lei, M. Hairston, and K. Drake (2011), Extreme Poynting flux in the dayside thermosphere: Examples and statistics, *Geophys. Res. Lett.*, doi:10.1029/2011GL048302, in press.

Korth, H., B. J. Anderson, H. U. Frey, and C. L. Waters (2005), High-latitude electromagnetic and particle energy flux during an event with sustained strongly northward IMF, *Ann. Geophys.*, *23*, 1295–2005.

Lavraud, B., A. Fedorov, E. Budnik, M. F. Thomsen, A. Grigoriev, P. J. Cargill, M. W. Dunlop, H. Rème, I. Dandouras, and A. Balogh (2005), High-altitude cusp flow dependence on IMF orientation: A 3-year cluster statistical study, *J. Geophys. Res.*, *110*, A02209, doi:10.1029/2004JA010804.

Li, W., J. Raeder, J. Dorelli, M. Øieroset, and T. D. Phan (2005), Plasma sheet formation during long period of northward IMF, *Geophys. Res. Lett.*, *37*, L12S08, doi:10.1029/2004GL021524.

Li, W., J. Raeder, M. F. Thomsen, and B. Lavraud (2008), Solar wind plasma entry into the magnetosphere under northward IMF conditions, *J. Geophys. Res.*, *113*, A04204, doi:10.1029/2007JA012604.

Onsager, T. G., J. D. Scudder, M. Lockwood, and C. T. Russell (2001), Reconnection at the high-latitude magnetopause during northward interplanetary magnetic field conditions, *J. Geophys. Res.*, *106*(A11), 25,467–25,488, doi:10.1029/2000JA000444.

Parker, E. N. (1996), The alternative paradigm for magnetospheric physics, *J. Geophys. Res.*, *101*(A5), 10,587–10,625, doi:10.1029/95JA02866.

Phan, T., et al. (2003), Simultaneous Cluster and IMAGE observations of cusp reconnection and auroral proton spot for northward IMF, *Geophys. Res. Lett.*, *30*(10), 1509, doi:10.1029/2003GL016885.

Raeder, J. (2003), Global magnetohydrodynamics: A tutorial, in *Space Plasma Simulation*, edited by J. Büchner, C. T. Dum, and M. Scholer, pp. 212–246, Springer, Berlin.

Raeder, J., J. Berchem, and M. Ashour-Abdalla (1998), The geospace environment modeling grand challenge: Results from a global geospace circulation model, *J. Geophys. Res.*, *103*(A5), 14,787–14,798, doi:10.1029/98JA00014.

Raeder, J., R. L. McPherron, L. A. Frank, S. Kokubun, G. Lu, T. Mukai, W. G. Paterson, J. B. Sigwarth, H. J. Singer, and J. A. Slavin (2001), Global simulation of the geospace environment modeling substorm challenge event, *J. Geophys. Res.*, *106*(A1), 381–395, doi:10.1029/2000JA000605.

Richmond, A. D. (2010), On the ionospheric application of Poynting's theorem, *J. Geophys. Res.*, *115*, A10311, doi:10.1029/2010JA015768.

Robinson, R. M., R. R. Vondrak, K. Miller, T. Dabbs, and D. Hardy (1987), On calculating ionospheric conductances from the flux and energy of precipitating electrons, *J. Geophys. Res.*, *92*(A3), 2565–2569, doi:10.1029/JA092iA03p02565.

Ruohoniemi, J. M., and R. A. Greenwald (1996), Statistical patterns of high-latitude convection obtained from Goose Bay HF radar observations, *J. Geophys. Res.*, *101*(A10), 21,743–21,763, doi:10.1029/96JA01584.

Strangeway, R. J., and J. Raeder (2001), On the transition from collisionless to collisional magnetohydrodynamics, *J. Geophys. Res.*, *106*(A2), 1955–1960, doi:10.1029/2000JA900116.

Tanaka, T. (2007), Magnetosphere-ionosphere convection as a compound system, *Space Sci. Rev.*, *133*, 1–72.

Trattner, K. J., S. A. Fuselier, S. M. Petrinec, T. K. Yeoman, C. Mouikis, H. Kucharek, and H. Reme (2005), Reconnection sites of spatial cusp structures, *J. Geophys. Res.*, *110*, A04207, doi:10.1029/2004JA010722.

Trattner, K. J., J. S. Mulcock, S. M. Petrinec, and S. A. Fuselier (2007), Probing the boundary between antiparallel and component reconnection during southward interplanetary magnetic field conditions, *J. Geophys. Res.*, *112*, A08210, doi:10.1029/2007JA012270.

Weimer, D. R. (1995), Models of high-latitude electric potentials derived with a least error fit of spherical harmonic coefficients, *J. Geophys. Res.*, *100*(A10), 19,595–19,607, doi:10.1029/95JA01755.

Weimer, D. R. (2001), An improved model of ionospheric electric potentials including substorm perturbations and application to the Geospace Environment Modeling November 24, 1996, event, *J. Geophys. Res.*, *106*(A1), 407–416, doi:10.1029/2000JA000604.

D. Knipp, High Altitude Observatory, National Center for Atmospheric Research, 3080 Center Green Dr., Boulder, CO 80302, USA. (knipp@ucar.edu)

J. Lei, Department of Aerospace Engineering Sciences, University of Colorado at Boulder, Boulder, CO 80309, USA. (jiuhou.lei@colorado.edu)

W. Li and J. Raeder, Space Science Center, University of New Hampshire, Morse Hall, 8 College Rd., Durham, NH 03824, USA. (wenhuil@unh.edu; j.raeder@unh.edu)